Quantum Monte Carlo method for the Bose-Hubbard model with harmonic confining potential

Yasuyuki Kato and Naoki Kawashima
Institute for Solid State Physics, University of Tokyo, 5-1-5 Kashiwa-no-ha, Kashiwa, Chiba 277-8581, Japan
(Received 30 June 2008; revised manuscript received 26 November 2008; published 5 February 2009)

We study the Bose-Hubbard model with an external harmonic field, which is effective for modeling a cold atomic Bose gas trapped in an optical lattice. We modify the directed-loop algorithm to simulate large systems efficiently. As a demonstration we carry out the simulation of a system consisting of 1.8×10^5 particles on a 64^3 lattice. These numbers are comparable to those in the pioneering experimental work by Greiner *et al.* [Nature (London) **415**, 39 (2002)]. Furthermore, we observe coherence between two superfluid spheres separated by a Mott insulator region in a "wedding-cake" structure.

DOI: 10.1103/PhysRevE.79.021104 PACS number(s): 05.30.Jp, 02.70.Ss, 02.70.Tt, 37.10.Jk

I. INTRODUCTION

Since the Mott transition was observed in an ultracold Bose gas trapped in an optical lattices [1], it has been a subject of active research [2–5]. Several theoretical investigations have been carried out for this system, such as quantum Monte Carlo (QMC) simulations of the Bose Hubbard model [6–10], which is effective for modeling optical lattice systems [11] and can describe the quantum phase transition [12]. Recently, Diener *et al.* [13] suggested that the temperature at which the experiments were carried out might not have been sufficiently low to allow the discussion of the quantum phase transition. Direct estimation of the temperature in the experiments is difficult and no figure has yet been given. A straightforward method of estimating the temperature is to compare the QMC simulation results for the momentum distribution with the results of the experiments. The systems are constructed from two types of potential: a periodic lattice potential and a harmonic trapping potential. The bosons are confined in a finite space by the harmonic trapping potential. In a typical experiment [1], the number of bosons is 2×10^5. To compare the experiments with the QMC simulations directly, it is necessary to simulate a system that contains the same number of lattice sites and bosons. The QMC based on the Feynman path integral is one of the most efficient presently used methods for dealing with such a large system. However, the simulation of a system whose size is comparable to that of the experiments was not published until recently: Gerbier *et al.* [10] include direct comparisons between the experiments and QMC simulations. In this paper, we demonstrate that such a simulation can be executed using a modified algorithm based on the directed-loop algorithm (DLA) [14,15] used in the QMC method. While the general principle of the DLA has very broad applicability, its straightforward application to boson systems is not efficient. Therefore, we accelerated the DLA by eliminating the problem of an excessive number of vertices. By adopting this improvement, the CPU time requirement was reduced greatly [16]. Even though we use the modified DLA, however, the simulation of such a large system is impossible because the required amount of computer memory is still too large. In this paper, we introduce a further modification of the DLA in Sec. III, and we demonstrate that it is possible to treat large systems using this method in Sec. IV A. Moreover, we provide evidence of the coherence between two superfluid regions separated by a Mott insulator region [17] in Sec. IV B. The coherence indicates the existence of effective coupling (Josephson coupling) between the two superfluid regions and that experimental optical lattice systems can have the same features as a Josephson junction.

II. MODEL AND DEFINITION OF MAIN PHYSICAL QUANTITIES

In this paper, we focus on a model of a cold atomic Bose gas trapped in an optical lattice. The effective model of the system is the one-band Bose-Hubbard model on a cubic lattice with an external harmonic field [6],

$$\mathcal{H} = -\frac{t}{Z}\sum_{\langle i,j\rangle}(b_i^\dagger b_j + b_i b_j^\dagger) + \frac{U}{2}\sum_i n_i(n_i-1) - \sum_i \mu_i n_i, \quad (1)$$

$$\mu_i = \mu_0 - \Omega|\boldsymbol{r}_i|^2, \quad (2)$$

where $b_i^\dagger$ (b_i) creates (annihilates) a particle at site i, $n_i = b_i^\dagger b_i$, $\langle i,j\rangle$ runs over all pairs of nearest-neighbor sites and $\boldsymbol{r}_i$ is the coordinate vector of site i with the origin being the center of the trapping potential. The symbols t, U, and μ_i denote the hopping amplitude, the on-site interaction between bosons, and the on-site external chemical potential, respectively. The coordination number in the cubic lattice is $Z=6$, and μ_0 is the value of the chemical potential at the center. We take the lattice spacing as our unit of distance.

We measure the local density ρ_i, momentum distribution $S(\boldsymbol{k})$, and local compressibility κ_i. They are defined as

$$\rho_i \equiv \frac{1}{\beta}\int_0^\beta d\tau\langle n_i(\tau)\rangle, \quad (3)$$

$$\kappa_i \equiv \frac{1}{\beta}\int_0^\beta\int_0^\beta d\tau' d\tau[\langle n_i(\tau)n_i(\tau')\rangle - \langle n_i(\tau)\rangle\langle n_i(\tau')\rangle], \quad (4)$$

$$S(\boldsymbol{k}) \equiv \sum_{i,j} e^{i\boldsymbol{k}\cdot(\boldsymbol{r}_i-\boldsymbol{r}_j)}\rho_{ij}, \quad (5)$$

where $\rho_{ij}\equiv\langle b_i^\dagger b_j\rangle$.

III. MODIFICATION OF DIRECTED-LOOP ALGORITHM

The QMC simulation is carried out by updating and sampling the world-line configurations based on the Feynman path integral using the Markov chain method. In the conventional DLA, we first place a few different types of scattering bodies called *vertices* all over space-time with densities depending on the diagonal element of the pair Hamiltonian. Next, we place a pair of discontinuities in space-time called a *worm* (one is called the *head* and the other is the *tail*) and let the head move around while changing the state. The head is always directed and changes its direction stochastically only when it meets a vertex. The scattering probability is entirely determined by the Hamiltonian. When the head meets the tail, the worm disappears and the Monte Carlo cycle is over. (See Refs. [14,15] for details.) As shown in our previous paper [16], the main reason for the inefficiency of the DLA for dilute bosonic systems is the excess number of vertices. The density of vertices is proportional to $Un_{\max}^2$, where $n_{\max}$ is the technical upper bound of the number of bosons. An increase in the number of vertices causes an increase in the frequency of the scattering. Then, the CPU time and computer memory required increase rapidly. In the previous paper, we eliminated this difficulty by a simple modification. The increase in the number of vertices is mainly caused by the U term in the Hamiltonian (1). The scattering at a vertex arising from the U term, which is a one-point scattering body on the world line, is very simple. That is, the head passes through the point or reverses its direction there. In the previous modification, we dealt with the U-term vertex by using a virtual placement. In short, the virtual placement was used to determine the next U-term vertex that changes the head's direction without actually placing the U-term vertices. Here, we further improve the DLA and apply the virtual placement to all the terms of the Hamiltonian (1). As discussed in Sec. V, our previous modification [16] is more effective than the present one for the purpose of reducing the CPU time. The improvement in this study is mainly to reduce the memory requirement. The principle underlying this modification is based on our previous modification.

We denote the vertex density and scattering probability as ρ_I and p_i^I, respectively. The index I indicates the type of interaction (e.g., a one-site interaction given by a U term or μ term or a two-site interaction given by a t term). The index i indicates the new direction of the head after scattering at a vertex (e.g., $i=0$ indicates that the head is scattered by the vertex and reverses direction; $i=1$ indicates that the head passes through the vertex). The values of ρ_I and p_i^I are calculated by following the procedure of the conventional DLA. The updating procedure of the present modified algorithm is as follows.

Step 1. Choose a point in the whole space-time uniformly randomly and place the worm at this point with the same probability as that of the conventional DLA. [See Fig. 1(a).]

Step 2. Focus on the interactions labeled I involving the site where the head is, and then focus on the region in front of the head where there is no kink interrupting the current site and the connected sites. (We consider only one-site and two-site interactions between nearest-neighbor sites. The focused area region is the shaded region in Fig. 1(b)). Then, calculate

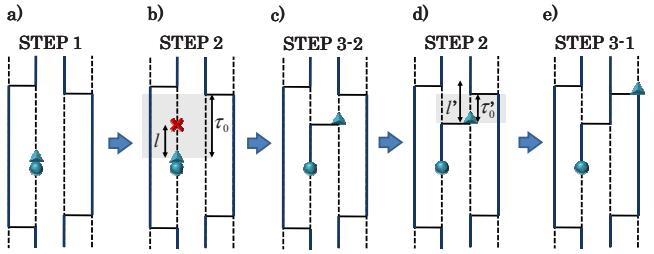

FIG. 1. (Color online) Motion of the head on the world-line configuration: the triangle and the circle represent the head and the tail of the worm, respectively. The lengthwise and crosswise directions indicate imaginary time and real space, respectively.

$$l = -\frac{1}{\varrho}\ln(1-R_1),$$

$$\varrho = \sum_I [\rho_I(1-p_1^I)], \tag{6}$$

using a uniform random number $R_1 \in [0,1)$, the vertex density ρ_I, and the probability p_1^I that the head passes through a vertex that represents the type I interaction. [See the Appendix for the derivation of Eq. (6).]

Step 3.1. If $l > \tau_0$, where τ_0 is the time length of the region under consideration in step 2, move the head by the distance τ_0 to the next kink. Then, choose the next direction of the head by following the conventional DLA. [In the case represented by Fig. 1(b), we only move the head by the distance τ_0 because the kink does not involve the current site.] Go to step 2. [See Figs. 1(d) and 1(e).]

Step 3.2. If $l \leqslant \tau_0$, using a uniform random number $R_2 \in [0,\varrho)$, choose an interaction I and a new direction $i(\neq 1)$ with probability proportional to $\rho_I p_i^I$. (See the Appendix.) Go to step 2. [See Figs. 1(b) and 1(c).]

When the head meets the tail again, the loop is closed and the worm disappears. After repeating this cycle several times, we sample a new world-line configuration. This algorithm, as a consequence, is a generalized version of the single-cluster loop algorithm [18]. In addition, it is similar to the worm algorithm [19]. In the worm algorithm, it is necessary to perform an integration using a local mean field when the worm moves. In this respect, the present algorithm is simpler than the worm algorithm.

The off-diagonal correlation function ρ_{ij} is related to the histogram of worm positions as in conventional DLA. [Refer to Eq. (10a) in Ref. [16] for the precise relationship between ρ_{ij} and the histogram.]

IV. DEMONSTRATIONS

A. Simulation of large system

Figure 2 shows the result of a simulation using the present algorithm as an illustration. The total number of bosons is 1.8×10^5 and the number of sites treated in the simulation is 64^3. Both are of the same order as those of typical experiments (e.g., the number of bosons and sites treated in experiments are 2.0×10^5 and $\sim 65^3$, respectively, in Ref. [1]). Fig-

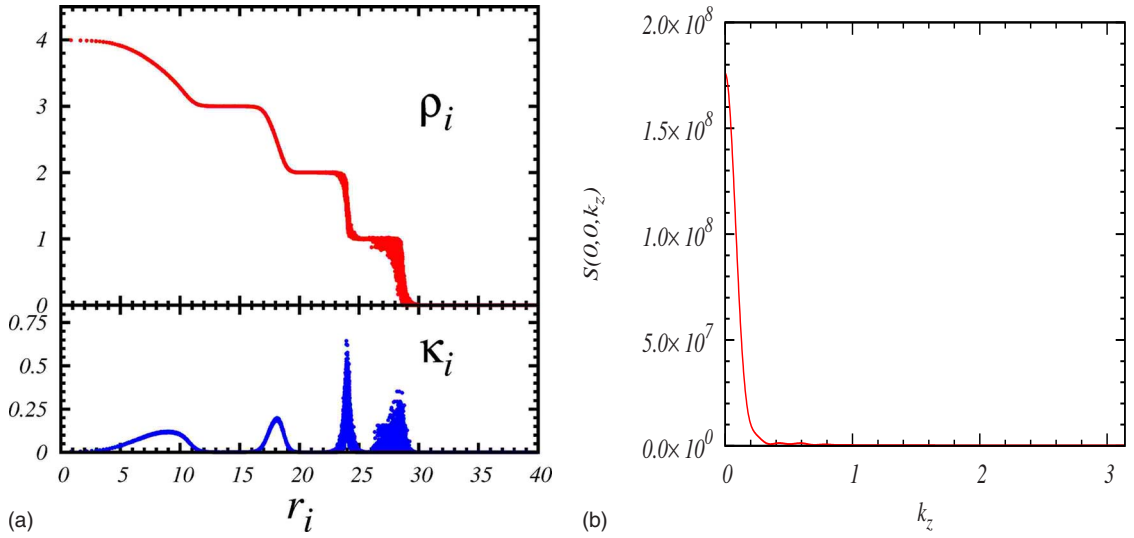

FIG. 2. (Color online) $U=20t$, $\mu_0=66t$, $\Omega=0.08t$, $\beta t=5.0$, and $n_{\max}=15$. The numbers of bosons and lattice sites are 1.8×10^5 and 64^3, respectively. (a) Local density of bosons and local compressibility as functions of r_i, where r_i is the distance from the center of the external chemical potential. (b) Momentum distribution of bosons.

ure 2(a) shows the local density of bosons ρ_i (top) and the local compressibility κ_i (bottom). The expected plateau at integral values of ρ_i and a large "wedding-cake" structure are observed. In addition, the expected peaks of κ_i appear in the regions between the plateaus. Figure 2(b) shows the momentum distribution function $S(\boldsymbol{k})$, which can be observed in experiments using the time-of-flight method.

B. Coherence between superfluid spheres

In this section, we consider the case where there are two concentric superfluid spheres whose radii are R_1 and R_2 $(R_1<R_2)$ separated by a Mott-insulator region as shown in Fig. 3(a). This situation can be realized by tuning the harmonic external chemical potential. An interesting question is whether these superfluid spheres are mutually coherent or incoherent. To answer the question, we calculate $\chi_{RR'}$ defined as

$$\chi_{RR'} \equiv \frac{1}{2N_R N_{R'}} \sum_{i\in R, j\in R', i\neq j} (\langle b_i^\dagger b_j\rangle + \langle b_j^\dagger b_i\rangle), \qquad (7)$$

where $\Sigma_{i\in R}$ denotes the sum over all sites whose distance from the center of the external chemical potential is R and $N_R \equiv \Sigma_{i\in R} 1$. Figures 3(b) and 3(c) show the results of simulations using the set of parameters shown in the caption of Fig. 3. The local densities ρ_i at a low temperature are shown in Fig. 3(b). It shows that the radii of superfluid spheres are $R_1 \simeq 12$, $R_2 \simeq 20$. We can observe coherent signals between the superfluid spheres at $\chi_{R_1R_2}$ and $\chi_{R_2R_1}$ in Fig. 3(c). The peaks at (R_1,R_1) and (R_2,R_2) in Fig. 3(c) indicate that the phases in the spheres with radii of R_1 and R_2 are coherent, respectively.

V. DISCUSSION

We first discuss the efficiency of the modified DLA. Figure 4(b) shows the node time required for the simulation using a node of an SGI Altix 3700 Bx2 system (Intel Itanium2 1.5 GHz) for three methods. The same number of Monte Carlo sweeps were executed for each method. The definition of a sweep is a set of Monte Carlo cycles (generating a worm and making a loop), in which the total traveling distance of the head is, on average, equal to the volume of space-time, βL^3. In Fig. 4(b), the node time for the present

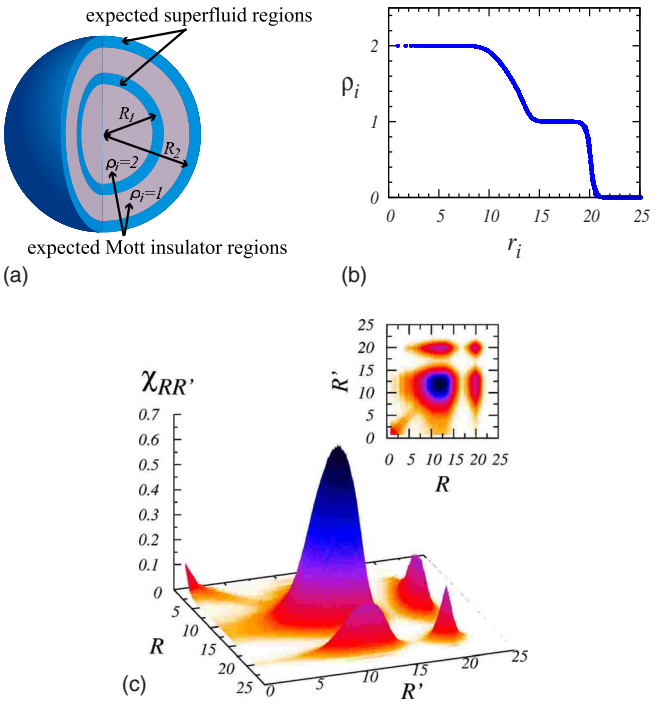

FIG. 3. (Color online) Low-temperature histogram of $\chi_{RR'}$. The parameters are $U/t=10$, $\mu_0/t=16$, $\Omega/t=0.039\,925\ldots$, $\beta t=20$, and $n_{\max}=12$, using cubic lattices whose numbers of sites are 42^3. (a) Expected real-space distribution of bosons at low temperature, (b) real-space distribution of bosons, and (c) histogram of $\chi_{RR'}$ as a function of R and R'.

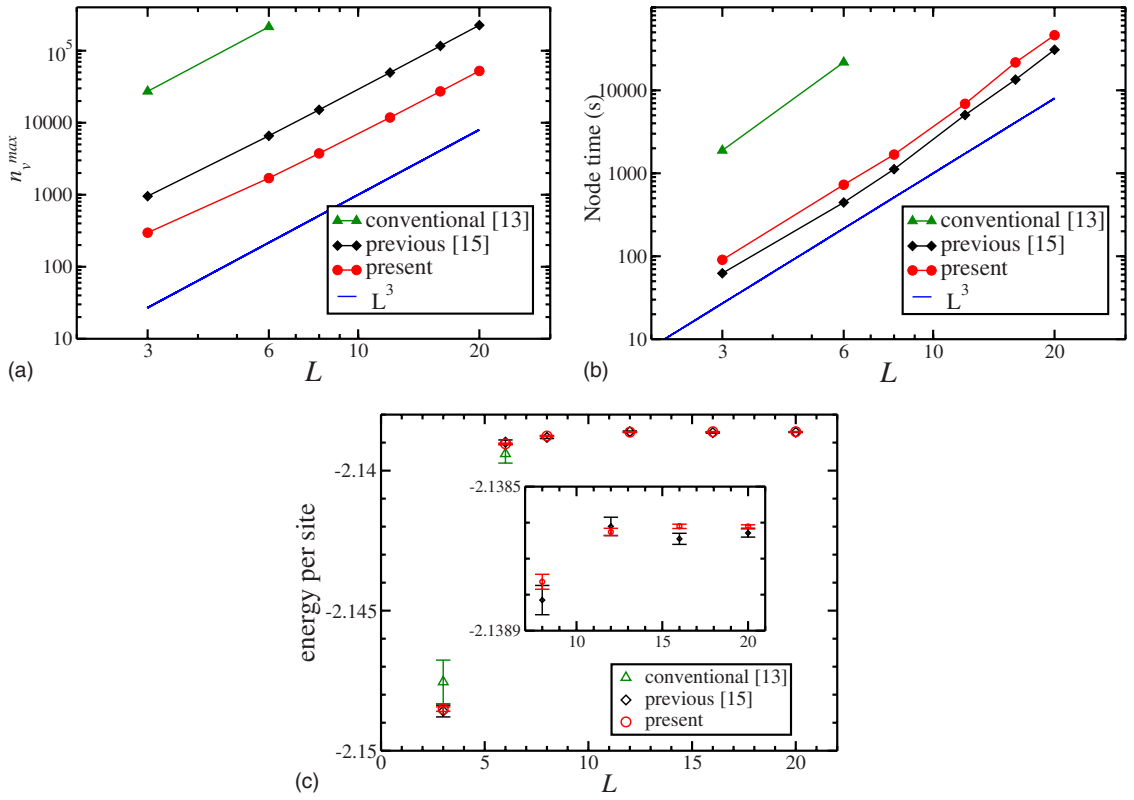

FIG. 4. (Color online) Comparison between the present algorithm, the previous modified DLA, and the conventional DLA. The parameters are chosen as follows: $t=1$, $t/U=0.25$, $\mu/U=0.5$, $\beta t=10.0$, $\Omega/t=0$ (homogeneous system), the maximum occupation number is $n_{\max}=8$, the number of sweeps for sampling is $n_{\mathrm{MCS}}=7000$, and the number of sweeps for equilibration is $n_{\mathrm{dump}}=3000$. The system used is SGI Altix 3700 Bx2 system (Intel Itanium2 1.5 GHz). We use one node with 64 CPUs, and parallel runs are executed. (a) Maximum number of vertices $n_v^{\max}$ per core, (b) node time (time of occupation of one node), and (c) energy per site $\langle \mathcal{H} \rangle / L^3$.

algorithm is roughly twice as long as that for the previous algorithm. On the other hand, the maximum number of vertices of the present algorithm is the least among the three methods as shown in Fig. 4(a). In other words, the memory usage of the present algorithm is the least among the three methods. Thus, the present algorithm better serves our present purpose of treating larger systems. In the conventional and previous DLA, vertices are placed even when there is no worm passing by. In the dilute limit, the difference between the previous and present algorithms becomes large. In addition, the generalization of the present idea to other cases where memory size limits the simulation scale is straightforward.

In Sec. IV A, we verified that the QMC simulation of a bosonic system whose size is comparable to that of experimental systems can be performed using our present method. Direct comparisons with experiments and the estimation of the temperature will be published elsewhere [20].

In Sec. IV B, we observed nondiagonal peaks of $\chi_{RR'}$ as a coherent signal between two superfluid spheres. This signal implies that the spheres are correlated with each other. It is therefore expected that the Josephson effect between the spheres can be observed dynamically [17]. In the case presented in this paper, at first, a diagonal peak at (R_1,R_1) appears as the temperature becomes low. When cooled further, the other diagonal peak at (R_2,R_2) and the nondiagonal peaks at (R_1,R_2) and (R_2,R_1) appear at the same temperature. We can understand this coincidence by considering the simpler case of the bilayered classical XY model with a weak interlayer coupling. Even if the interlayer coupling is very small comparing with the intralayer coupling, these two layers are synchronized in the thermodynamic limit because the huge number of spins makes the effective total coupling between the two layers large. As a result, the two layers become coherent as soon as each layer orders. The number of spins corresponds to the number of coherent bosons belonging to the superfluid spheres in the present case. The system is completely confined in a finite volume. Therefore, in general it can happen that the diagonal peak and nondiagonal peaks appear at different temperatures because the number of coherent bosons is too small.

ACKNOWLEDGMENTS

The present work was financially supported by a MEXT Grant-in-Aid for Scientific Research (B) (No. 19340109), a MEXT Grant-in-Aid for Scientific Research on Priority Area "Novel States of Matter Induced by Frustration" (No. 19052004), a Grant-in-Aid for JSPS Fellows, and by the Next Generation Supercomputing Project, Nanoscience Program, MEXT, Japan. The simulations were carried out at the Supercomputer Center, Institute for Solid State Physics, University of Tokyo.

APPENDIX: VIRTUAL PLACEMENT OF VERTICES

In this appendix, we derive Eq. (6) by considering the virtual placement of vertices. In the update process of the conventional DLA, the head typically passes through several vertices before it is scattered by a vertex. In the virtual placement process, we place vertices only where they scatter the head. We also show that the new direction and location of the head are determined stochastically using a uniform random number $R \in [0, \varrho)$. In Appendix A of Ref. [16], we discussed the virtual placement of one-site vertices arising from the U term. In this paper, we extend the virtual placement to all types of vertices. In the conventional DLA, the vertices are placed according to a Poisson distribution. That is to say, the probability that n_v vertices are placed in a uniform interval whose length is τ_0 is

$$P_{n_v}(\rho\tau_0) = \frac{(\rho\tau_0)^{n_v}}{n_v!} e^{-\rho\tau_0}, \tag{A1}$$

where ρ is the vertex density, which is determined by the properties of the Hamiltonian.

In Fig. 1(b), for example, there are four types of interaction to be considered for the motion of the head: the one-site interaction between bosons on the same site (U term), the external chemical potential corresponding to the one-site interaction (μ term), and the two-site interactions of the boson hopping to a neighbor on the right and the left (t term). We consider the probability that the head passes through all vertices placed in an imaginary time interval x and changes its direction at a vertex of interaction type I_1 placed in an infinitesimal time window dx. The probability is

$$P_{I_1}(x)dx = \left[\prod_{I'} \left(\sum_{n_v=0}^{\infty} P_{n_v}(\rho_{I'}x)(p_1^{I'})^{n_v} \right) \right] \times [\rho_{I_1}dx][1 - p_1^{I_1}], \tag{A2}$$

where $p_1^{I'}$ is the scattering probability that the head passes through the type-I' vertex in the conventional DLA. The first factor is the probability of the head traveling a distance x without being scattered by any type of vertex. The second is the probability of finding a vertex of interaction I_1 in the interval x to $x+dx$. The third is the probability that the head changes its direction at the vertex. Then, the probability that the head changes its direction in the interval x to $x+dx$ is derived as

$$P(x)dx = \sum_{I_1} P_{I_1}(x)dx = \varrho e^{-\varrho x}dx, \tag{A3}$$

where $\varrho \equiv \Sigma_I(1-p_1^I)\rho_I = \Sigma_I(\Sigma_{i\neq 1}p_i^I)\rho_I$. According to the probability distribution $P(x)$, the distance l that the head travels without scattering is stochastically chosen using Eq. (6). In addition, the probability that the scattering takes place at a type-I_1 vertex is

$$\frac{\left(\sum_{i\neq 1} p_i^{I_1}\right)\rho_{I_1}}{\varrho}. \tag{A4}$$

The new direction of the head is selected with a probability proportional to the scattering probability of the conventional DLA, i.e., p_i^I. We therefore determine the type of interaction and the new direction of the head stochastically using only a uniform random number $R \in [0, \varrho)$ after determination of the distance l.

[1] M. Greiner, O. Mandel, T. Esslinger, T. W. Hänsch, and I. Bloch, Nature (London) **415**, 39 (2002).
[2] I. Bloch, Nat. Phys. **1**, 23 (2005).
[3] M. Greiner, O. Mandel, T. W. Hänsch, and I. Bloch, Nature (London) **419**, 51 (2002).
[4] F. Gerbier, A. Widera, S. Fölling, O. Mandel, T. Gericke, and I. Bloch, Phys. Rev. A **72**, 053606 (2005).
[5] B. Paredes, A. Widera, V. Murg, O. Mandel, S. Fölling, I. Cirac, G. V. Shlyapnikov, T. W. Hänsch, and I. Bloch, Nature (London) **429**, 277 (2004).
[6] V. A. Kashurnikov, N. V. Prokof'ev, and B. V. Svistunov, Phys. Rev. A **66**, 031601(R) (2002).
[7] S. Wessel, F. Alet, M. Troyer, and G. G. Batrouni, Phys. Rev. A **70**, 053615 (2004).
[8] S. Wessel, F. Alet, S. Trebst, D. Leumann, M. Troyer, and G. G. Batrouni, J. Phys. Soc. Jpn. **74**, 10 (2005).
[9] L. Pollet, C. Kollath, K. V. Houcke, and M. Troyer, New J. Phys. **10**, 065001 (2008).
[10] F. Gerbier *et al.*, Phys. Rev. Lett. **101**, 155303 (2008).
[11] D. Jaksch, C. Bruder, J. I. Cirac, C. W. Gardiner, and P. Zoller, Phys. Rev. Lett. **81**, 3108 (1998).
[12] M. P. A. Fisher, P. B. Weichman, G. Grinstein, and D. S. Fisher, Phys. Rev. B **40**, 546 (1989).
[13] R. B. Diener, Q. Zhou, H. Zhai, and T.-L. Ho, Phys. Rev. Lett. **98**, 180404 (2007).
[14] O. F. Syljuåsen and A. W. Sandvik, Phys. Rev. E **66**, 046701 (2002).
[15] N. Kawashima and K. Harada, J. Phys. Soc. Jpn. **73**, 1379 (2004).
[16] Y. Kato, T. Suzuki, and N. Kawashima, Phys. Rev. E **75**, 066703 (2007).
[17] S. Vishveshwara and C. Lannert, Phys. Rev. A **78**, 053620 (2008).
[18] B. B. Beard and U. J. Wiese, Phys. Rev. Lett. **77**, 5130 (1996).
[19] N. V. Prokof'ev, B. V. Svistunov, and I. S. Tupisyn, JETP **87**, 310 (1998).
[20] Y. Kato, Q. Zhou, N. Kawashima, and N. Trivedi (unpublished).